Molecular Therapy
Methods & Clinical Development
Original Article

Transcriptomics-informed pharmacology identifies epigenetic and cell cycle regulators that enhance AAV production

Joshua Tworig,[1] Francis Grafton,[1] Kaylin Fisher,[1] Markus Hörer,[2] Christopher A. Reid,[1] and Mohammad A. Mandegar[1]

[1]Ascend Advanced Therapies CA, Inc, Alameda, CA 94501, USA; [2]Ascend Advanced Therapies GmbH, 82152 Planegg, Germany

Recombinant adeno-associated virus (rAAV) is a widely used viral vector for gene therapy. However, these vectors have limited availability due to manufacturing challenges with productivity and quality. These challenges can be addressed by better understanding the mechanisms that influence cellular responses during rAAV production. In this study, we aimed to identify targets that may enhance rAAV production using transcriptomic analyses of five cell lines with variable capacities for rAAV production. Using an intersectional approach, we measured the transcriptional responses of these cells during rAAV production and compared transcriptional profiles between high and base producers to identify possible targets for enhancing production. During rAAV production, we found transcriptional differences in cell cycle and nucleosome components contributed to proliferative capacity and DNA replication. We also saw upregulation of several core functions, including transcription, stress response, and Golgi and endoplasmic reticulum organization. Conversely, we saw consistent downregulation of other factors, including inhibitors of DNA-binding proteins and mitochondrial components. With a drug-connectivity analysis, we identified five classes of drugs that were predicted to enhance rAAV production. We also validated the efficacy of histone deacetylase and microtubule inhibitors. Our data uncover novel and previously identified pathways that may enhance rAAV production and quality to expand availability of rAAV for gene therapies.

INTRODUCTION

Adeno-associated viruses (AAVs) are nonpathogenic, single-stranded DNA viruses that are widely used for *in vivo* gene delivery. Recombinant AAVs (rAAVs) have gained popularity in the gene therapy field due to their well-established safety profile, broad and tunable tropism, and nonpathogenic nature.[1,2] As of 2024, seven rAAV gene therapies have been approved and are commercially available.[3,4] Several programs are in late-stage clinical development, and hundreds are in earlier stages of development.[5,6] However, given the promise of curative rAAV therapies, gene therapy developers require high doses of vectors, especially for systemically delivered AAVs. Also, there is growing emphasis on enhancing the quality of rAAV vectors through reducing plasmid- and host-derived impurities and partially packaged vectors.[7,8] Yet, these efforts have been hindered by challenges with rAAV production and manufacturing at scale.

Current methods of rAAV production result in relatively low volumetric yields, estimated at 1,000- to 4,000-fold lower than monoclonal antibody production.[8] This low yield may be due to inefficient manufacturing processes related to our limited biological understanding of cell-based rAAV production. rAAV molecules are complex and require careful assembly of 60 protein subunits to form the capsid and then incorporate a single-stranded DNA molecule.[9–11] The low yield may also be related to cell-based biomanufacturing platforms[12,13] that often use cells outside of their evolutionary context as biologic-production factories. As a result, current off-the-shelf production platforms may not push rAAV production beyond the physiologic limits of unmodified cells. Also, the rAAV production process requires precise kinetics of expression and stoichiometric ratios of replicase (Rep) and capsid (Cap) helper elements.[14] Rep expression induces cell cycle arrest,[15] and the helper gene E4 activates the stress and DNA damage response, resulting in apoptosis.[16] Furthermore, during viral replication and assembly, rAAV production is limited by activation of host-cell defense and antiviral response pathways,[7] as well as other unknown molecular barriers.[11,14] By better understanding and eliminating these challenges, we could enhance the efficiency of viral replication and assembly.

To further understand pathways that are altered during rAAV production, we analyzed RNA expression patterns over time using five HEK293 cell lines. We hypothesized that by identifying dysregulated pathways during rAAV production and studying transcriptional differences between base and high producer cell lines, we could uncover valuable targets that enhance AAV production.

Received 24 June 2024; accepted 14 November 2024;
https://doi.org/10.1016/j.omtm.2024.101384.

Correspondence: Mohammad A. Mandegar, Ascend Advanced Therapies CA, Inc, Alameda, CA 94501, USA
E-mail: Mandegar@gmail.com

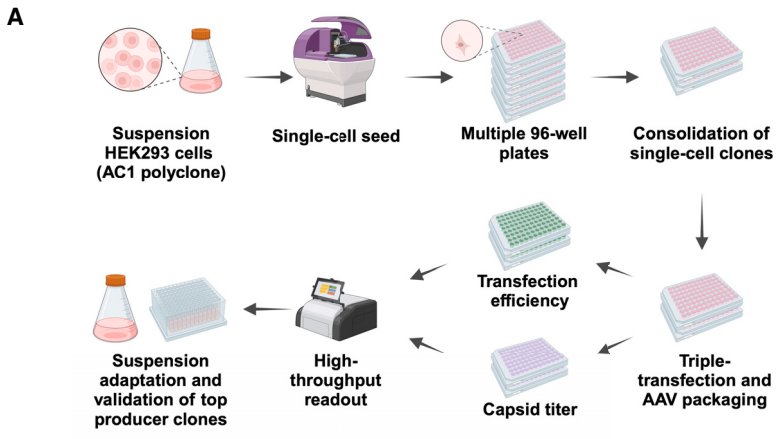

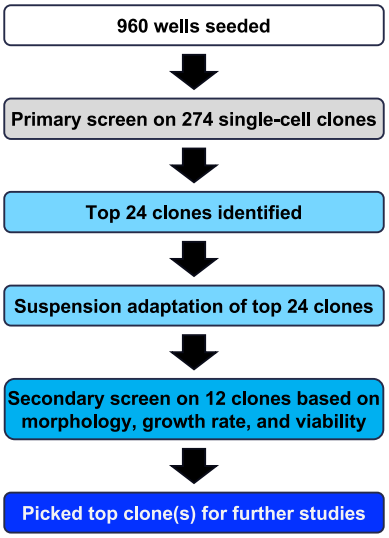

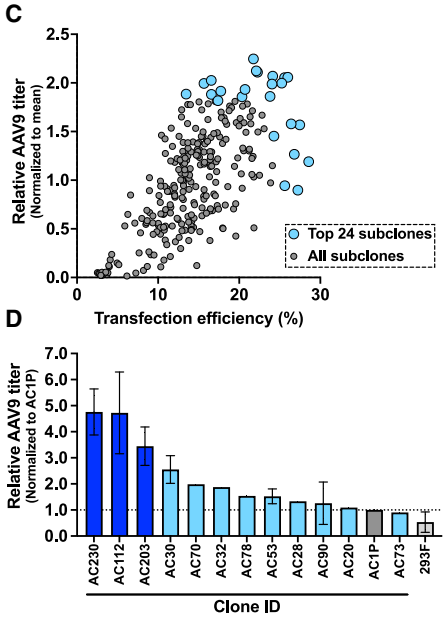

Figure 1. Clonal cell line generation with improved AAV9 yields

(A) Schematic of workflow for single-cell cloning and isolation of HEK293 clones with improved AAV production capacity. The Solentim VIPS single-cell seeder was used to isolate clonal HEK293 cells using a two-step clonality verification process. (B) Subclone selection strategy for identifying the top AAV9 producer clonal cells. (C) Approximately 300 single-cell-derived HEK293 clones were identified based on growth. The 24 top-performing colonies were selected based on transfection efficiency and AAV9 production. (D) After suspension adaptation, AAV productivity of the best suspension-adapted clones was measured relative to AC1P (parental polyclonal cell line). n = 1–2 replicates per cell line. Data are shown as mean ± SD fold-change from AC1P (control).

RESULTS

Generation of clonal cell lines with greater AAV9 yields

To identify robust and widely applicable transcriptional changes during AAV9 production, we used HEK293 cells from two separate sources: Expi293F (“293F” for short) from Thermo Fisher Scientific and HEK293 cells (“AC1P” for short) from Cytion (Table S1). First, standard AAV production protocols were developed using triple-plasmid transfection in both 293F and AC1P cells (Figures S1A and S1B). The same transfection protocol was used for both cell lines. See Figure S1C for typical transfection rates based on flow cytometry. Then, cell growth, cell viability, and AAV9 capsid titer were monitored for 10 days after transfection (Figures S1D–S1F).

To identify cell clones with higher AAV production potential, we isolated clonal cell lines from AC1P (polyclonal) cells using the Solentim VIPS (Verified In-Situ Plate Seeding) single-cell seeder (Figures 1A and 1B). During seeding and colony growth, clonality was ensured with a double-imaging system (once at droplet dispense and again at whole well imaging; Figure S1G). Approximately 300 clonally derived AC1P colonies were screened for transfection efficiency and AAV9 production in adherent culture format (Figure 1C). Based on these parameters, the top 24 clones were selected to convert to suspension format for further development and characterization. Among these clones, transfection efficiency averaged 14.4% ± 5.3%. (Figure 1C). The relatively low transfection efficiencies in this initial screen were possibly due to the growth format and handling of the cells before transfection, as well as the underestimate of the true transfection efficiency via imaging (see materials and methods; compare with Figure S1C). During the suspension-adaptation phase, the cell viability and growth rate of these clones were measured (Figures S1H and S1I). After a 9-day suspension-adaptation phase, the top 12 clones were selected based on cell growth and viability, and then expanded in 125-mL shake flasks for secondary screens of AAV9 production. Several clonal cell lines showed greater AAV9 production than the 293F and AC1P parental lines (Figure 1D).

Cell line selection and RNA-seq experimental design

Of the clonal cell lines, we selected the top three AAV producers (AC230, AC112, AC203; Figure 1D) for transcriptomic analysis alongside 293F and AC1P (Table S2). Each of these lines underwent triple-plasmid transfection in 125-mL shake flasks. Samples for RNA-seq analysis were collected before transfection (0 h) and during AAV9 production (24 and 72 h after transfection) (Figure 2A). The AAV9 vector genome (vg) titer of these samples was measured at 72 h after transfection (Figure 2B). Next, to identify genes associated with different AAV yield phenotypes, we classified cell lines into two categories: “base” producers (293F and AC1P) and “high” producers

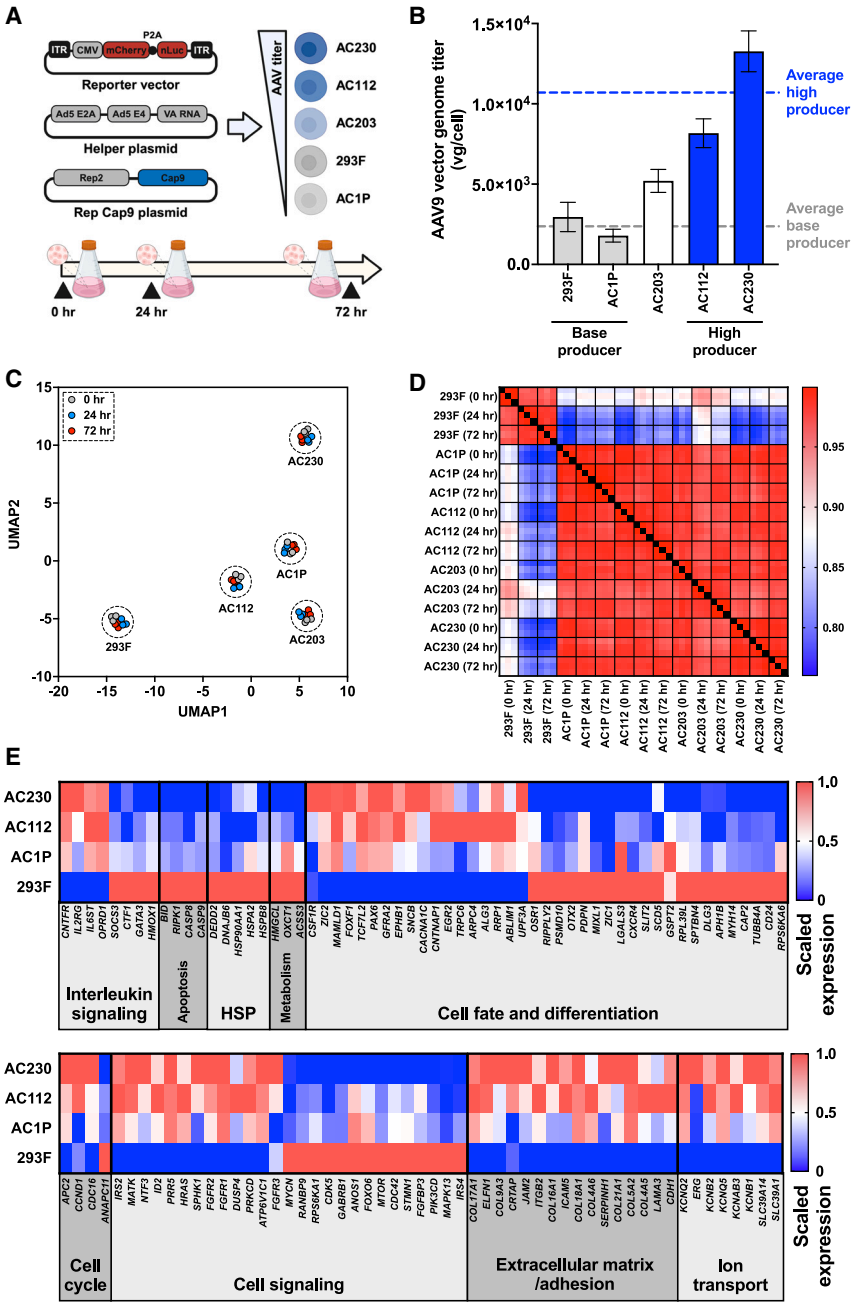

Figure 2. RNA-sequencing experimental strategy and top differentially expressed gene sets for high vs. base AAV producer cell lines

(A) Workflow and experimental design for RNA-sequencing analysis during AAV production. The 293F, AC1P (polyclonal cell line), and three clonally derived cell lines from AC1P were used for the analysis. Samples were collected at 0 h (hr; before transfection) and at 24 and 72 h after triple-plasmid transfection. Three small-scale shake flasks were used per condition. (B) The AAV9 vector genome titer of all five cell lines was measured at 72 h. The 293F and AC1P cells were designated as "base producers" with an average titer of approximately 2.4E9 vg/mL. AC112 and AC230 were designated as high producers with an average titer of approximately 1.1E10 vg/mL. $n = 3$ replicates per cell line. Data are shown as mean ± SD. (C) Uniform manifold approximation and projection (UMAP) and (D) gene correlation matrix of the five HEK293 cell lines show high reproducibility among replicates. RNA expression differences between cell lines are greater drivers of variability than differences between timepoints after transfection. (E) Heatmap of differentially enriched genes and functional categories in higher AAV producer cells (AC230 and AC122) vs. base producer cells (AC1P and 293F). Differentially enriched transcripts were manually categorized into cell cycle modulators, cell signaling, extracellular matrix/adhesion, ion transport, mitochondrial, heat-shock protein (HSP), and cell fate and differentiation.

(AC112 and AC230). To keep the analysis balanced, the AC203 cell line (mid-producer) was excluded from this comparison. Base producers yielded an average of approximately 2.4E3 vg/cell and high producers yielded an average of approximately 1.1E4 vg/cell (Figure 2B).

The bioinformatics workflow on raw data and quality control parameters are outlined in Figures S2A–S2C. Uniform manifold approximation and projection (UMAP), as well as RNA expression correlation analyses, indicated high reproducibility among replicates (Figures 2C and 2D). UMAP-based clustering suggested that transcriptional differences between cell lines were greater drivers of variability than differences between timepoints after transfection (Figure 2C). Correlation analysis revealed that 293F cells exhibited notable divergence in expression profiles from AC1P, AC112, AC203, and AC230 (Figure 2D). We expected this result because the latter three clonal lines were all derived from the AC1P parental line. This result also suggests that any differential expression between high and base producers could be driven by the 293F line, which is reflected in a series of pairwise differential expression analyses between all cell lines (Figure S2D).

RNA-seq analysis identifies differentially expressed pathways associated with improved AAV production

To identify gene expression patterns associated with improved AAV production, we compared gene expression patterns among the high producers (AC230, AC112) and base producers (AC1P, 293F) before transfection (0 h) (Figure 2B). Between the base and high producers, 801 genes were differentially expressed ($|\log_2$ [fold-change]$| > 0.5$; adjusted p value <0.05). Of those genes, 327 were significantly upregulated and 474 were significantly downregulated in high producers (Table S3).

To identify significantly enriched and depleted pathways in high vs. base producers, we performed Reactome pathway analysis using the full list of differentially expressed genes.[17] We found that these genes commonly influence pathways that regulate the cellular stress response (interleukin signaling, apoptosis, heat shock), cell state (cell fate and differentiation, cell cycle), extracellular matrix/adhesion organization, and ion transport. We hypothesize that one or more of these pathways may contribute to enhanced AAV production in AC230 and AC112 (Figure 2E).

Because the expression profile of the 293F cell line was notably different from the other four cell lines (Figures 2D and S2D), we performed an additional differential expression analysis without the 293F cell line (comparing the AC1P parental line vs. the two high producers AC112 and AC230). The same significance and fold-change thresholds were applied for this analysis (adjusted $p < 0.05$; $|\log2\text{fold-change}| > 0.5$). Approximately 44% of the 289 differentially expressed genes identified in this analysis overlapped with those reported in Figure 2E (293F included) (Figure S2F). Next, we performed gene ontology analysis using the list of 289 differentially expressed genes. Overrepresented ontological groups that overlapped with the analysis reported in Figure 2E included signaling, cell differentiation, extracellular matrix, and adhesion-related groups (Figure S2G). These results highlight the importance of cell line choice in RNA-seq experiments.

AAV production is associated with transcriptional modulation of cell state, signal transduction, homeostasis, and extracellular interactors

We further analyzed the subset of time-dependent expression differences that were shared among all five cell lines during AAV production. We identified genes that were differentially expressed at 24 and 72 h after transfection vs. before transfection (0 h). At 24 h, 499 genes were differentially regulated, of which 228 were significantly upregulated and 271 were significantly downregulated. At 72 h, 542 genes were differentially expressed, of which 481 were significantly upregulated and 61 were significantly downregulated (Figure S2E and Table S3).

With manual pathway analysis of differentially expressed genes, we uncovered an array of fundamental host-cell processes that were altered during AAV production. Some of these processes overlap with those uncovered with the Reactome pathway analyses (Figure 2E). Notably, among the top upregulated genes during AAV production, several were involved in cell fate and differentiation (e.g., *CELSR3, TNFRSF12A, LIF*), signal transduction (e.g., *INHBE, AMH, TNFRSF9*), cell cycle regulation (e.g., *GADD45B, CEND1, NABP1*), protein homeostasis (e.g., various heat shock protein family members), and transcriptional activation (e.g., *FOSB, ETV4, ETV5, RELB, MYB*). Among the most significantly downregulated factors were negative regulators of transcription (e.g., *ID1, ID2, ID3*) and extracellular matrix/cell adhesion molecules (e.g., *HAS2, COL3A1*) (Figures 3A–3D).

Recent transcriptional studies implicated many of the same pathways and processes that we identified in AAV production, despite variations in study design, including plasmid and cell sources, transfection conditions, and growth media (Table S1). For example, Wang et al.[18] identified several upregulated stress-response and homeostatic genes that align with our data, including *HBB*, *HSPA6*, and *CCL5*, as well as genes that encode microtubule-interacting proteins *STMN4* and *DNAH17* (Figures S3A–S3C). Also, Chung et al.[7] reported transcriptional upregulation of nucleosome assembly, inflammatory, viral response, and histone genes during AAV production. We observed similar trends in our dataset, with significantly higher nucleosome assembly and histone genes and, with a few exceptions, slightly higher inflammatory response and virus defense genes at 72 h (Figures S3D–S3F). We detected activation of only a handful of upstream regulators of differentially expressed genes reported by Chung et al.[7] (Figure S3G).

Intersectional analysis reinforces involvement of transcription, cell proliferation, and extracellular matrix organization in AAV production

Ultimately, we aimed to identify genes that were both involved in AAV production and associated with higher AAV production. To this end, we analyzed the intersect between genes that were (1) modulated during AAV production and (2) differentially expressed between high and base AAV producer cells. For this analysis, we first identified all unique genes that were either upregulated or downregulated between any two timepoints during AAV production. Second, we identified genes that were either upregulated or downregulated at all timepoints (before transfection and at 24 and 72 h after transfection) in high AAV-producing cell lines. This analysis identified 1,143 unique genes that were modulated during AAV production. Of these genes, 110 were upregulated and 245 were downregulated in high producers at all timepoints (Table S5).

Next, we aimed to identify targets that may enhance AAV production in HEK293 cells. To this end, we analyzed the intersect between differentially expressed genes during AAV production (1,143) and those that were upregulated (110) and downregulated (245) in high producer cells (Figure 3E). The genes that were differentially expressed during AAV production and upregulated in high producers included regulators of proliferation (*BTNL9, EMX2OS, MATK, RASSF1*), transcription factors (*RELB, ZNF692*), and nuclear pore complex components (*NPIPB6, NPIPB9*). The genes that were differentially expressed during AAV production and downregulated in high producers included viral DNA-targeting cytosine deaminases (*APOBEC3B/C*), positive regulators of proliferation (*CDK5, MFAP2, PTGIS, RAB3B, TNFRSF12A*), and stress-response genes (*GSTO2, HMOX1, HSPB8, IFI6*). Also, genes for several cell adhesion and extracellular matrix molecules were modulated during AAV production and upregulated (*CDH23, COL17A1, COL18A1, JAM2, TNXB*) or downregulated (*BCAM, COL4A5, COL4A6, COL5A2*) in high producer cells.

A model for AAV production based on coordinated regulation of multiple cellular processes

To better understand the regulatory events that underlie AAV production, we identified several cellular processes that were significantly

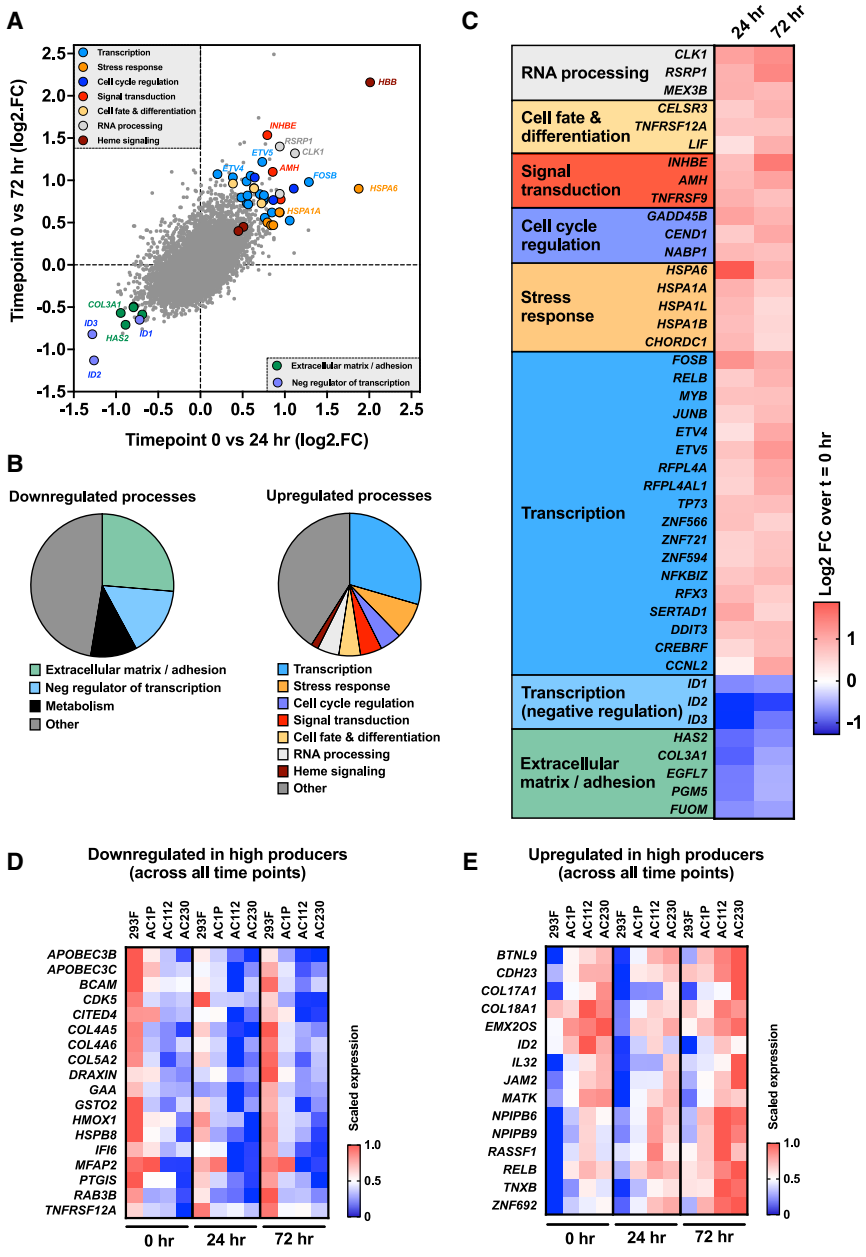

Figure 3. RNA sequencing reveals modulation of transcription, protein homeostasis, signal transduction, and cell cycle regulation during AAV9 production

(A) Scatterplot comparing fold-change gene expression at 0 h (hr; before transfection) vs. 72 and 24 h during AAV production. Data averaged from all five cell lines and three replicates per time point. Several gene families and genes of interest are highlighted. (B) Pathway analysis of differentially expressed genes shows upregulated transcripts represent transcription factors, heat shock proteins, signal transduction molecules, cell cycle regulators, and heme signaling molecules. Other upregulated processes include microtubule destabilizers, Golgi organization, and vesicle transport. Downregulated transcripts include inhibitors of DNA-binding and extracellular matrix proteins. (C) Heatmap of most significant differentially expressed genes at 24 and 72 h during AAV production. Data averaged from all five cell lines and three replicates per time point. Color scale represents $\log_2$ (fold-change) expression from before transfection. (D and E) Heatmaps of the intersection of genes modulated during AAV production with genes downregulated (D) and upregulated (E) in high AAV producer cell lines. Color scale represents $\log_2$ (counts per million), averaged across replicates and normalized from 0 to 1 for each gene. neg, negative.

upregulated and downregulated based on a gene ontology (GO) analysis. Among the most significantly downregulated GO terms were glutathione-related processes, suggesting a role for oxidative stress in AAV production. Other significantly downregulated GO terms included mitochondrial processes (particularly electron transport), nicotinamide-adenine dinucleotide (NADH) dehydrogenase, and respiratory chain complex I. Collagen fibril organization was also significantly downregulated, further implicating the importance of extracellular interactions in AAV production. Conversely, the most significantly upregulated GO terms included amino acid transport, stress response, RNA polymerase activity, endoplasmic reticulum stress, and Golgi cisterna membrane components (Figures 4A and 4B). Other upregulated GO terms included nuclear pore complex and histone components, reflecting the importance of nuclear transport and viral DNA replication during AAV production (Figure 4B).[19,20]

Within each of these GO terms, we categorized the list of differentially expressed genes at 72 h after transfection. Aligned with the upregulated transcriptional activators (Figures 3C and 3D), we saw strong and coordinated downregulation of inhibitors of DNA-binding genes (*ID1, ID2, ID3*). We also saw downregulation of negative regulators of transcription, including *MAFB* and *SMAD6* (Table S4). Further, we saw coordinated downregulation of subunits comprising the proteasome (e.g., *PSMD9*, *PSMA6*) and the mitochondrial ribosomal proteins and electron transport chain. This finding suggests broad downregulation of protein turnover and energy production pathways during AAV production (Figures 4C and S4A). We also saw upregulation of genes involved in amino acid transport (e.g., *SLC3A2*, *SLC1A3*), Golgi (e.g., *GOLGA8A*, *GOLGA8B*), nuclear pore complex (e.g., *NPIPA1*, *NPIPB9*), and nucleosome assembly (e.g., *H1-2*, *H2BC5*) (Figures 4D and S4B). These findings highlight that a cellular transition from oxidative energy production to biomolecular synthesis may be important for AAV production. Interestingly, we found opposing regulation of two cytoskeletal

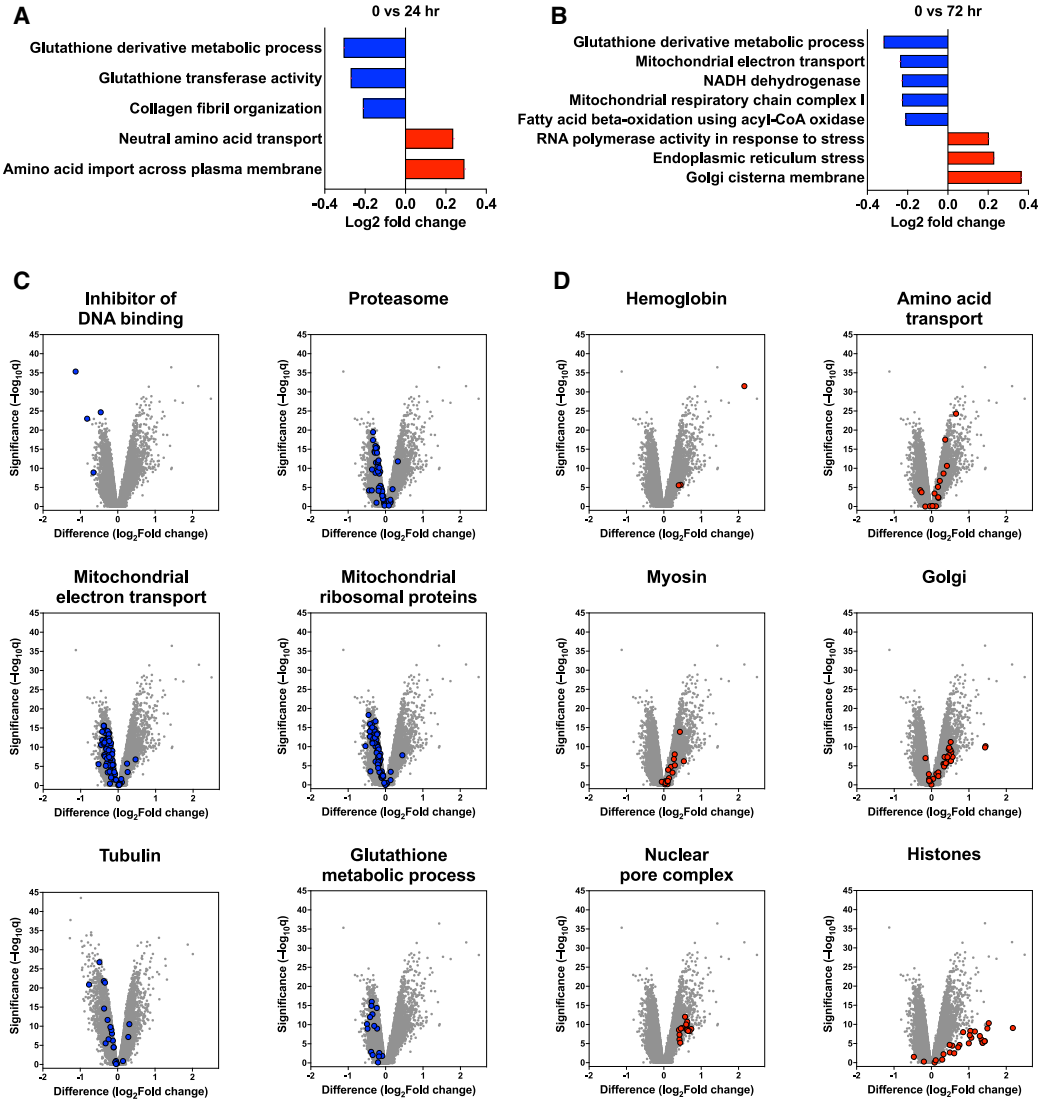

(legend on next page)

components: tubulin, which was generally downregulated, and myosin, which was generally upregulated. This finding suggests that specific cytoskeletal rearrangements may support intracellular transport of viral particles during AAV production.

Based on these results, we constructed a simple model of activated and repressed pathways during AAV production (Figure 4E). This model proposes specific cellular processes that may be targeted for perturbation with the goal of enhancing AAV production for therapeutic use.

Drug-connectivity analysis identifies cell cycle and epigenetic modulators that enhance AAV9 production

We leveraged our RNA-seq data to identify targets that could be pharmacologically modulated to enhance AAV production. To this end, we developed a workflow and triaging strategy to identify putative pharmacological enhancers of AAV production (Figure S5A). We performed two sets of analyses: one that included the 293F cell line and one that excluded it. In both analyses, we identified enriched and depleted targets or mechanisms of action during AAV production. Approximately 1,000 compounds were predicted to modulate the enriched pathways. This primary list was filtered to include only annotated drugs with putative biological targets with a $p < 0.01$ and a normalized enrichment score (NES) greater than 1.3 or less than −1.3. The analysis that included the 293F cell line predicted 266 drugs, while the analysis excluding the 293F cell line predicted 292 drugs to modulate the enriched pathways. Of these, 180 drugs were shared between the two analyses (Figure S5A). Both analyses shared over 85% identity in enriched and depleted targets and mechanism of action during AAV production. Examples of enriched targets and pathways included protein synthesis and tubulin polymerization, whereas depleted pathways included histone deacetylases (HDACs) and cell cycle and cell signaling kinases (Figures 5A, 5B, and S5B–S5G).

We focused on the 266 annotated compounds predicted to modulate pathways during AAV production from the 293F-inclusive analysis. Among the list of triaged compounds, 62 were available in our small-molecule screening library.[21] These compounds target the cell cycle, cell signaling, DNA replication and synthesis, HDACs, ion channels, protein homeostasis, and tubulin. These 62 compounds were tested at 1-μM dose and screened for AAV9 capsid titer in 239F cells (Figure 5C).

Among the 62 compounds, 12 increased AAV9 production 1.5-fold above baseline (approximately 19% hit rate), and three increased AAV9 production 3-fold above baseline (approximately 5% hit rate). Then, we validated these results using the top two most well-defined target classes, HDACs and microtubules, in the top AAV producer line (AC230). For these studies, HDAC and microtubule inhibitors were first added at a single dose at the time of transfection in AC230 cells. These inhibitors led to an AAV9 capsid titer up to approximately 2- to 3-fold higher than with dimethyl sulfoxide (DMSO) control (Figures S5H and S5I). In a follow-up study, a subset of these inhibitors was tested at three doses in AC230 cells, and AAV9 vector genome titers were measured using qPCR. The AAV9 vector genome titers were up to 1.8-fold higher with HDAC inhibitors and up to 3.2-fold higher with microtubule inhibitors than with DMSO (Figure 5D).

DISCUSSION

In this study, we combined transcriptional analysis with pharmacological perturbations to improve our mechanistic understanding of key pathways involved in AAV production. We analyzed five HEK293 cell lines with varying capacities for AAV production and used RNA-seq to identify genes and pathways that are (1) modulated during AAV production and (2) differentially expressed between base and high AAV producers. Using this intersectional strategy, we identified a subset of novel and known pathways that are differentially expressed in host cells and could be targeted to enhance AAV production.

We identified core cellular functions that were upregulated and downregulated during AAV production. The upregulated functions included transcriptional activation, cellular stress responses, signal transduction, and cell cycle regulation. Conversely, the downregulated functions included mitochondrial ribosomal and electron transport components, proteasomal proteins, glutathione metabolic process modulators, and transcriptional repressors. Many of these processes were differentially expressed between base and high AAV-producing cell lines. Using these results, we developed a general cellular model for AAV production that is characterized by a complex shift in cell state, with widespread modulation of energy production and biosynthesis.

For the key pathways we identified in our study, we used drug-pathway interaction analysis to predict, triage, and test the effects of pharmacologic modulators of altered pathways during AAV production. We tested a subset of these predicted compounds, and up to 19% of them improved AAV production 1.5-fold above baseline. This improvement is a substantially higher hit rate than if we had performed an unbiased high-throughput screen, which has typical hit

Figure 4. Selection of differentially expressed cellular components and processes incorporated into a model for AAV production

(A and B) Gene ontology term analysis at 24 h (hr) (A) and 72 h (B) reveals downregulation of mitochondrial, collagen, and glutathione and fatty acid metabolic processes during AAV production. Significantly upregulated GO categories include amino acid transport, stress response, and Golgi cisterna components. (C) Volcano plots of select processes reveal coordinated downregulation among inhibitors of DNA-binding, proteasome, mitochondrial electron transport, mitochondrial ribosomal proteins, tubulin, and glutathione metabolic process genes during AAV production. (D) Volcano plots of select processes reveal coordinated upregulation among hemoglobin, amino acid transport, myosin, Golgi, nuclear pore complex, and nucleosome assembly genes during AAV production. (E) Model of activated and repressed pathways during AAV production points to targets that could be modulated to enhance AAV yield and quality. NADH, nicotinamide-adenine dinucleotide.

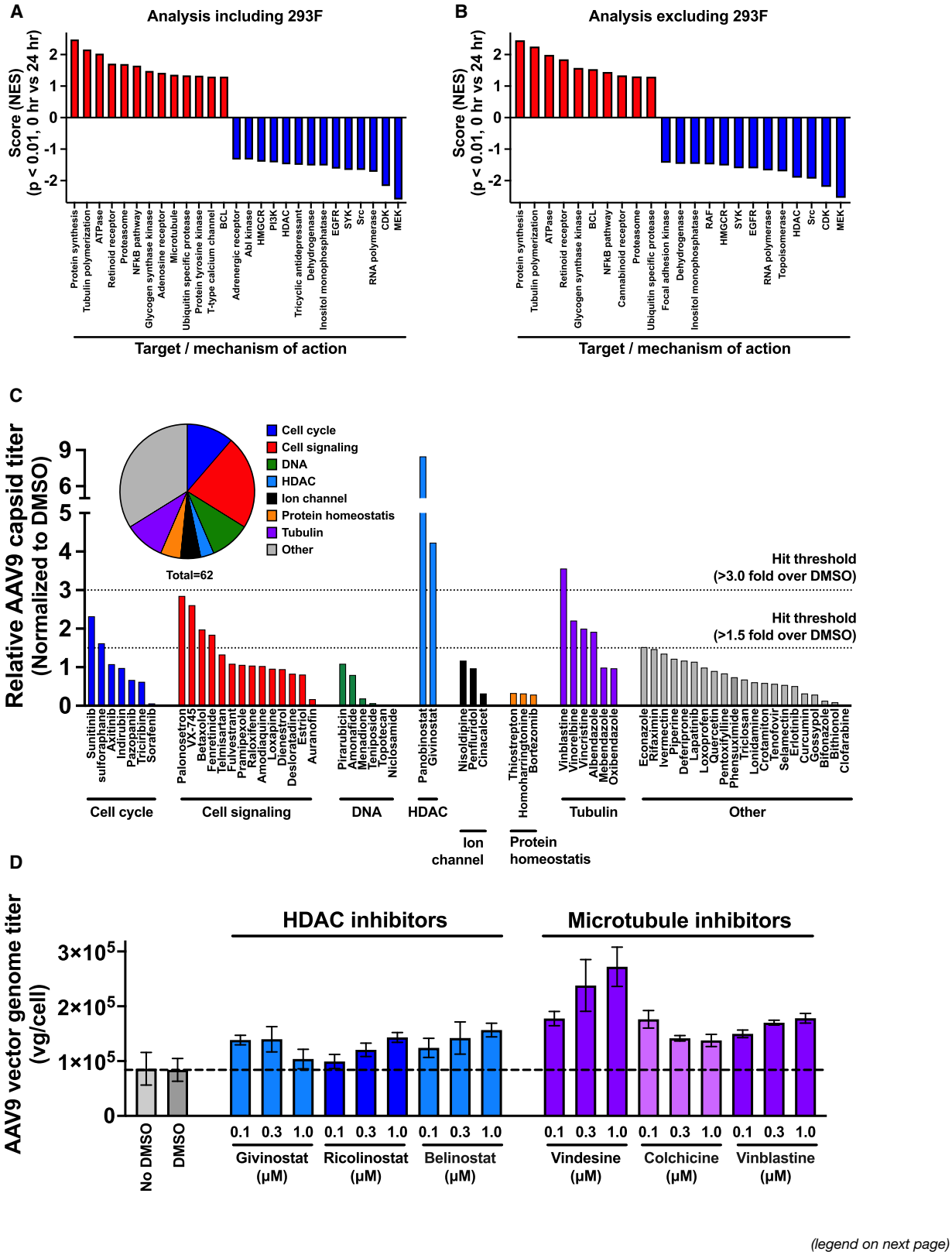

(legend on next page)

rates that range from 0.1% to 1%.[22–24] These findings support that, when seeking to improve viral production, selectively screening compounds with a transcriptomics-informed strategy has a higher success rate than a hypothesis-free approach. We further justified our approach by identifying and validating HDAC and microtubule inhibitors as enhancers of AAV production. Our findings support that targeting epigenetics, activating transcriptional machinery, and modulating the cell cycle are important mechanisms in promoting AAV production.

AAV production via plasmid transfection is associated with a broad range of transcriptional responses in the host cell. For example, transfection results in modulation of transcription that is generally short-lived and returns to baseline by 24 h after transfection.[7] During AAV production, transcriptional machinery in the host cell must produce both viral proteins and host-cell proteins involved in downstream homeostatic responses. This duality was evident in our data that showed upregulation of many transcription factors during the mid-late phase of AAV production. These upregulated factors included *ETV4* and *ETV5*, which bind to the enhancer of the adenovirus E1A gene and act as transcriptional activators.[25] The upregulated factors also included *FOSB, RELB,* and *MYB*, which are known proto-oncogenes that control proliferation and cell differentiation.[26–28]

Transcriptional upregulation of histones has also been reported during AAV production.[7] These findings support that epigenetic modulation of transcriptional machinery is a key mechanism in enhancing viral replication and production. We and others have shown that HDAC inhibitors can increase AAV[29,30] and lentivirus production.[31] This increase is likely due to the capacity of HDAC inhibitors to stimulate viral gene transcription through chromatin remodeling.[32]

We observed a coordinated downregulation of negative regulators of transcription during AAV production. These negative regulators included genes that encode inhibitors of the DNA-binding proteins *ID1, ID2, ID3*, *MAFB,* and *SMAD6*, which may hinder viral replication. *ID* isoforms also may modulate cell growth, senescence, and differentiation.[33] *MAFB* represses erythroid genes, including the transferrin receptor that is essential for heme synthesis.[34] This finding aligns with our observed upregulation of *HBB* during AAV production. *SMAD6* acts as a transcriptional corepressor to inhibit bone morphogenetic protein signaling in the nucleus via a negative feedback loop.[35,36] Also, *SMAD6* downregulation may be a compensatory response to reduced *ID1, ID2,* and *ID3,* which are downstream effectors of bone morphogenetic protein signaling.[37,38]

We observed opposing regulation of proliferative genes involved in AAV production. Specifically, we saw a general upregulation of inhibitors of proliferation and downregulation of enhancers of proliferation among high AAV producers. These findings reflect that AAV production is heavily influenced by phases of the cell cycle, with AAV most effectively produced during the S/G2 phase.[39] This finding, coupled with a coordinated upregulation of histones during AAV production (also reported by Chung et al.[7]), is characteristic of the S phase of the cell cycle, when viral DNA replication is most efficient.[40,41] We also saw opposing regulation of tubulin and myosin during AAV production, with tubulin isoforms generally downregulated and myosin isoforms upregulated. Tubulin and myosin are involved in mitotic spindle formation and, thus, affect cell cycle progression and proliferation.[42,43] Myosin may also be used to transport viral cargo during AAV production.

One way to boost AAV titers is to modulate the cell cycle. For example, AAV titers were increased by arresting cells in the G2/M phase using microtubule inhibitors (e.g., nocodazole).[29] Also, AAV titers were increased in a gain-of-function screen using both CRISPR (clustered regularly interspaced short palindromic repeats) activation and transgene overexpression of spindle and kinetochore associated complex subunit 2 (SKA2), and inositol 1, 4, 5-trisphosphate receptor interacting protein (ITPRIP) increased AAV titer altering the host cell cycle to increase replication of the AAV vector genome.[22] In addition, temperature shifts that synchronize the cell cycle can improve AAV[44] and adenovirus[45] production. Further, a slower rate of cell growth may be beneficial during AAV production, because it reduces the rate of plasmid loss and dilution.[14] Reducing cell growth can also divert less cellular machinery to host-cell DNA replication, and protein synthesis, thereby freeing cellular resources for vector amplification, replication, and capsid assembly.

In our cell lines, AAV production was associated with widespread modulation of various signaling pathways, including kinases and other elements involved in growth factor signaling. Notably, mitogen-activated protein kinases (MAPKs) are crucial signaling molecules that regulate cell cycle, differentiation, and apoptosis.[46,47] During AAV production, MAPK activity was negatively regulated.[7] Also, dysregulation of MAPK signaling using miR-431 and miR-636 improved AAV2 assembly and potency by >3-fold.[48] These

Figure 5. Pathway analysis identifies druggable pathways that may be modulated to enhance AAV production

Normalized enrichment score (NES) analysis of targets and mechanism of action during the early stages of AAV production (0 vs. 24 h [hr]). (A) Analysis including 293F cells and (B) analysis excluding 293F cells, with p values <0.0, were used to identify enriched and depleted pathways. Examples of enriched pathways included protein synthesis and tubulin polymerization, whereas depleted pathways included histone deacetylases (HDACs) and various classes of kinases (mostly involved in the cell cycle and cell signaling). (C) Data from 62 drugs that were tested at 1-μM doses and screened for fold-increases in AAV9 capsid titers vs. dimethyl sulfoxide (DMSO) controls in the 293F line. Among the 62 drugs, 12 increased AAV9 production 1.5-fold above baseline (approximately 19% hit rate), whereas three increased AAV9 production 3-fold above baseline (approximately 5% hit rate). (D) Validation studies using HDAC and microtubule inhibitors applied at three doses at the time of transfection in the top producer cell line AC230. The AAV9 vector genome titer was up to 1.8-fold greater with HDAC inhibitors and up to 3.2-fold greater with microtubule inhibitors than DMSO control. $n = 3$ replicates per treatment. Data are shown as mean ± SD. MEK, mitogen-activated protein kinase kinase; PI3K, phosphoinositide 3-kinase; SYK, spleen tyrosine kinase.

findings underscore the intricate interplay between cell cycle regulation and signaling pathways during AAV production and may offer strategies to enhance AAV vector yields.

During viral production, cells undergo cellular stress that evokes an array of responses via heat shock, unfolded protein response (UPR), oxidative stress, and immune response pathways.[7,18,49–51] Based on our data, some of the most significantly upregulated transcripts during AAV production were heat-shock proteins (HSPs), including HSPA6, HSPA1A, HSPA1L, HSPA1B, and the HSP90 co-chaperone CHORDC1. HSPs can be activated by viral infection and may suppress viral replication, or they may be modulated by the virus itself to promote its replication.[51,52] Also, HSP expression may be upregulated during AAV replication due, in part, to a large influx of immature proteins into the endoplasmic reticulum and Golgi complex, thus evoking a UPR. This possibility is supported by our dataset that showed modulation of transcription factors that affect UPR, including ATF6B and several CREB-related factors (Table S4).[53,54]

Oxidative stress due to mitochondrial damage[50] can also upregulate hemoglobin.[55] In alignment with this finding, we observed upregulated *HBB*, *HBA1*, and *HBA2* at 24 and 72 h after transfection (Figure S4). Conversely, *HMOX1* (*heme oxygenase I*) was significantly downregulated during AAV production and in our high AAV producers. *HMOX1* is a stress-response gene, and its product catalyzes the degradation of heme, an important cofactor of hemoglobin and various enzymes.[56] The byproducts of heme degradation include scavengers of reactive oxygen species, which have anti-inflammatory effects and can inhibit viral replication.[57]

Inhibiting stress-response pathways and apoptosis may also improve viral yields. For example, interferons may activate the innate immune response and apoptotic pathways during AAV production.[7,18] Also, inhibiting interferon signaling with ruxolitinib (JAK1-TYK2 inhibitor) blocks JAK-STAT signaling and can double AAV yields in low-producing cell lines.[58] In addition, double-knockout of two key regulators of apoptosis (*BAX* and *STAT1)* in HEK293 cells increased AAV5 titers by 1.8-fold.[59] In line with these findings, our high AAV-producing cell lines showed downregulation of genes encoding other key apoptotic factors, including *BID, CASP8,* and *CASP9*. These downregulated genes could enable AAV-producing cells to survive under greater stress associated with AAV production.[60]

Our study had a few notable limitations. First, although our differential expression results during AAV production align with recent reports,[18,61] we did not analyze gene expression under non-virus-producing conditions. Thus, we could not account for changes in expression that result from changes in culture vessel or transfection alone. Second, most commercially available libraries of bioactive compounds predominantly contain anti-cancer drugs that either directly or indirectly affect the cell cycle. Because the scope of our search space is limited by the diversity of the chemical space, we could not probe all possible influential pathways and targets. Third, we initially screened small molecules at a fixed, single dose (1 μM), which limited our ability to identify compounds that are efficacious above or below this concentration. Fourth, variability in gene expression patterns among different HEK293 cell lines suggest that our findings may not be universally applicable to all cellular production systems. This limitation is especially relevant when using different plasmid systems, media formulations, feed strategies, and transfection reagents. Finally, our results may have been confounded by using bulk RNA-seq, which can obscure the heterogeneity within the transfected cell population. Cells that successfully take up all three plasmids and produce AAV likely exhibit distinct expression profiles when compared with those that take up fewer or no plasmids. A recent study using single-cell RNA-seq during AAV production has shown that nearly half of the transfected cells lack expression of at least one plasmid, with only 8% of the cells showing high mRNA levels for all three plasmids. Additionally, only 2.5% of the transfected cells were shown to have intracellular capsids assembled, highlighting the inefficiency and cellular heterogeneity of transfection-based rAAV production.[62] Hence, future research could expand the range of targetable pathways by optimizing compound dosage; implementing genetic screens via CRISPR-Cas9, small interfering RNA, and transgene overexpression; and performing single-cell RNA-seq to focus on cells that successfully produce AAV. Additionally, a fluorescence-activated cell sorting approach could be employed to isolate an enriched population of transfected cells to provide more relevant transcriptomic data and overcome the limitations of bulk RNA-seq analysis. These optimizations will be crucial for translating our hypotheses into practice and effectively scaling up from a laboratory setting to large-scale bioreactor systems.

In conclusion, our study elucidates the complex transcriptional and cellular responses involved in AAV production. By integrating pathway analysis and pharmacologic screening, we showed that targeted modulation of specific pathways, such as transcriptional regulation and cell cycle control, can enhance AAV production. Our study also highlights the power of transcriptional profiling to identify genes and pathways as targets for cell and process engineering to improve rAAV production for clinical applications. These findings expand our mechanistic understanding of AAV production and highlight potential targets for enhancing the efficiency of viral replication and assembly to advance AAV production processes.

MATERIALS AND METHODS

Information on cell lines, media, compounds, and kits used in this study are listed in Table S2.

Adherent cell culture and suspension adaptation of HEK293 cells

Adherent HEK293 cells were expanded in Dulbecco's modified Eagle's medium (DMEM), high glucose, GlutaMAX Supplement, pyruvate (Thermo Fisher Scientific, Waltham, MA) supplemented with 10% fetal bovine serum (FBS) (Thermo Fisher Scientific, Waltham, MA) in a 37°C, 5% CO_2 incubator. Once cells reached approximately 80% confluency, the media was carefully aspirated and replaced with Expi293 expression medium (Thermo Fisher Scientific, Waltham,

MA). Then the cells were incubated for 48 h in the adherent format at 37°C, 5% CO_2. After 48 h of cell adaptation to Expi293 expression media, cells were resuspended in 2 mL fresh media and placed on an orbital shaker (125 rpm, 19 mm orbital throw) in a 37°C, 5% CO_2 incubator. After 2 days of suspension adaptation, cell viability and density were measured using a Countess 3 and Trypan Blue (Thermo Fisher Scientific, Waltham, MA), and cells were maintained at 0.5–5 E6/mL. All cell lines were negative for mycoplasma based on the MycoAlert Mycoplasma Detection Kit (Lonza, Cambridge, MA).

Maintenance of HEK293 cells in suspension before transfection

Suspension HEK cells were maintained in Expi293 expression medium on an orbital shaker (125 rpm, 19 mm orbital throw) in a 37°C, 5% CO_2 incubator. Cell growth and viability were monitored for 7–10 days until cells had reached a density of 2.5–5E6/mL and >95% viability before transfection. Cells were then centrifuged at 500 × *g* for 5 min. Spent media was aspirated, and the cell pellet was resuspended in the appropriate volume of Expi293 expression medium to achieve a density of 2.5E6/mL in a 30-mL shake flask.

Clonal cell line generation and screening

To generate and screen clonal cell lines for enhanced AAV production, AC1P cells were resuspended to 9,500 cells/mL in DMEM, high glucose, GlutaMAX Supplement, pyruvate (without FBS) after ensuring >90% viability. Single-cell seeding was carried out in Corning Costar 96-well flat-bottom cell-culture-treated plates (cat. number 3596, Corning, NY) using the Solentim VIPS apparatus according to the recommended instructions. Each seeded well was imaged immediately after seeding, before filling the well with DMEM +10% FBS. After seeding all wells, wells were imaged again using the "verify clonality" function. This imaging was repeated each day for 5 days. Starting on day 5, wells were imaged using the "monitor colony growth" function. This imaging was repeated every other day until about 2 weeks after seeding.

Once colonies reached 65%–80% confluence, they were consolidated into new 96-well plates if they exhibited clear evidence of clonality (a single colony derived from a single cell at the time of seeding). The consolidation plates were then distributed among three sister plates for expansion, transfection, and cryopreservation. Transfection plates were pre-treated with fibronectin (1:1,000 in phosphate-buffered saline [PBS]; STEMCELL Technologies, Cambridge, MA) before transferring clonal colonies. Transfection efficiency during the clonal cell line generation process was determined by imaging each well 48 h after transfection. Quantification of the percentage of GFP-positive cells was performed using Cytation 5 microscope (BioTek Instruments, Winooski, VT) at ×10 magnification.

AAV harvest and purification

The triple transfection system uses a pHelper plasmid, a RepCap9 plasmid, and an inverted terminal repeat (ITR)-containing reporter plasmid. The pHelper plasmid contains Ad5 E4, Ad5 E2A, and Ad5 VA-RNA. The RepCap9 plasmid expresses AAV2-derived Rep78 and Rep68 under control of the P5 promoter; Rep52 and Rep40 under control of the P19 promoter; and VP1, VP2, and VP3 derived from AAV9 under control of the P40 promoter. The ITR-containing reporter plasmid includes mCherry-P2A-nanoluciferase (NLuc) driven by a cytomegalovirus (CMV) promoter. After transfecting cells using TransIT-VirusGEN (Mirus Bio, Madison, WI), cells were allowed to produce AAV for up to 72 h before harvesting samples for titer analysis. Cells were lysed via three rounds of freezing on dry ice followed by thawing at 37°C. After mixing lysed samples, cell debris was removed by centrifuging at 1,000 × *g* for 10 min. Then AAV-containing supernatant was saved for processing and stored at −80°C.

Determination of capsid titer using ELISA

A streptavidin-coated high-capacity plate (Thermo Fisher Scientific, Waltham, MA) was coated for 1 h at room temperature with the CaptureSelect Biotin anti-AAV9 conjugate (Thermo Fisher Scientific, Waltham, MA) at a dilution of 1:10,000 in PBS + 0.1% Tween 20 (PBST). After incubation, the capture antibody solution was aspirated from each well of the plate, and each well was washed three times with 150 μL PBST. Then 100 μL of either standard or sample was added to the plate. A 5- to 7-point standard was used in all studies with the AAV9 empty capsid standard (Progen, Heidelberg, Germany). The plate was covered with foil-sealing film and incubated on a shaker for 1 h at room temperature. After incubation, the entire sample was aspirated, and the plate was washed three times with 150 μL PBST. CaptureSelect horseradish peroxidase anti-AAV9 conjugate (Thermo Fisher Scientific, Waltham, MA) was diluted 1:50,000 in PBST and 100 μL of the diluted detection antibody was added to each well. The plate was covered with foil-sealing film and incubated on a shaker for 1 h at room temperature. After incubation, the horseradish peroxidase anti-AAV9 conjugate solution was aspirated and washed three times with 150 μL PBST. Then 100 μL TMB ELISA (enzyme-linked immunosorbent assay) substrate (highest sensitivity; Abcam, Waltham, MA) was added per well and incubated for 2–5 min before adding 100 μL of ELISA Stop Solution (Thermo Fisher Scientific, Waltham, MA). Absorbance was measured on the Varioskan microplate reader at 450 nm (Thermo Fisher Scientific, Waltham, MA).

Determination of vector genome titer using qPCR

Purified or crude viral supernatant was treated with DNase I for 90 min at 37°C according to the manufacturer's instructions (New England BioLabs, Ipswich, MA). Then qPCR was performed using a custom FAM probe against Nano Luciferase (Thermo Fisher Scientific, Waltham, MA) and TaqMan Fast Advanced Master Mix (Thermo Fisher Scientific, Waltham, MA) on a QuantStudio 6 Flex real-time PCR system (Thermo Fisher Scientific, Waltham, MA). Plasmid DNA was used from a concentration of 0.0001–1 ng/μL to generate a standard curve.

RNA preparation and sequencing

For each cell line and replicate, 2.5E6 cells were removed before transfection (0 h), as well as 24 and 72 h after transfection. Cells were pelleted, flash frozen, and stored at −80°C. Total RNA was extracted using the Direct-zol-96 RNA Kit (Zymo Research, Irvine, CA) according to

the manufacturer's instructions. RNA concentration was quantified using a NanoDrop spectrophotometer (Thermo Fisher Scientific, Waltham, MA), and RNA quality was assessed via High-Sensitivity RNA Screen Tape Analysis (Agilent [Santa Clara, CA]; performed via SeqMatic [Fremont, CA]). Illumina stranded mRNA library preparation and sequencing (NovaSeq V1.5, S1, 100 cycles) were performed by SeqMatic (Fremont, CA). On average, 42,271,540 ± 7,224,160 reads (100-base pair, single-end) were generated per sample. All RNA-seq data were deposited on the Gene Expression Omnibus (GEO) database: GEO Submission (GSE269485).

Differential expression analysis

The quality of sequence reads was assessed using FastQC[63] and reads were aligned to the human genome (GRCh38.110) using Hisat2[64] to the human genome (GRCh38.110). After generating genomic alignments, the Subread's featureCounts function was used to generate gene-level read counts.[65] On average, Hisat2 aligned 95.6% ± 1.9% of reads to the genome one or more times, and 97.8% ± 1.2% of these reads were successfully assigned to genomic features.

After obtaining high-quality sequence alignments and counts, an expression matrix was generated and submitted to the BigOmics platform for differential expression analysis.[66] Raw counts were converted into counts per million (CPM) and $\log_2$ normalized for downstream analysis. Protein-coding genes with at least 1 CPM across two or more samples were included in the analysis. By default, the BigOmics platform uses a combination of statistical tests for differential expression via DESeq2 (Wald), edgeR (QLF), and limma (trend).

Initial UMAP clustering and differential expression analyses were performed within the BigOmics web environment and exported for visualization. Pairwise gene expression correlations between samples were calculated in R using the Pearson method. Multiple contrasts were generated in the BigOmics environment to compare expression profiles (1) across cell lines, (2) among AAV titer phenotypes, and (3) after transfection timepoints. Unless otherwise noted, a false discovery rate (FDR) threshold of 0.01 and a $\log_2$ (fold-change) threshold of 0.5 were applied to identify top differentially expressed genes across analyses. First, to compare expression profiles across cell lines (Figures 2 and S2), we generated (1) contrasts using pairwise combinations of all five cell types (293F, AC1P, AC112, AC203, and AC230) and (2) a matrix to compare the number of differentially expressed genes between each pair. Then differential expression tests were performed between the base and high AAV-producing groups. Finally, to identify genes that were significantly upregulated or downregulated during AAV production, pairwise differential expression tests were performed among the 0-, 24-, and 72-h time points after transfection.

GO and drug-interaction analysis

To identify sets of coregulated genes associated with high AAV-producing cells, Reactome pathway analysis was performed using the top differentially expressed genes between base and high-producing cell lines.[17] Overrepresented pathways were identified by using a p value threshold of 0.05. The results were then manually curated for heatmap visualization by combining overlapping pathways into broader categories and removing duplicate genes across categories (Figure 2D). A similar approach was carried out to classify differentially modulated genes during the AAV production time course. Also, GO analysis was performed using the BigOmics platform to identify significantly enriched cellular components and molecular functions during AAV production (Figure 4).

An L1000 drug-connectivity analysis was performed within the BigOmics platform using genes that were differentially expressed between 0 and 24 h and between 0 and 72 h.[67] NES with p values <0.01 were used to identify enriched and depleted targets, mechanisms of action, and drug candidates at 24 and 72 h after transfection.

Compound screening

Compounds were solubilized in DMSO at a 10-mM stock concentration, and later diluted to the appropriate concentration (0.1–1.0 μM in 0.1% DMSO). The control condition was 0.1% DMSO. Microplates or shake flasks were then incubated at 37°C and 5% CO_2 for 72 h with no media change before sample harvest.

Statistical analysis

The number of replicates is indicated in the figure legends. Unless otherwise specified, Student's t test was used for statistical analysis, with significant differences defined as $^{*}p < 0.05$, $^{**}p < 0.01$, $^{***}p < 0.001$, $^{****}p < 0.0001$. Error bars indicate standard deviation (SD).

DATA AND CODE AVAILABILITY

Our RNA-seq data has been deposited on the GEO database: GEO Submission (GSE269485).

ACKNOWLEDGMENTS

This project was supported by Ascend Advanced Therapies. We thank C.R. Herron for editing the manuscript. We thank H. Griffiths and R. Feitzinger, L. Leveque-Eichhorn, and I. Ukani for assay optimization and plasmid cloning. Illustrations were created with BioRender.com.

AUTHOR CONTRIBUTIONS

F.G., C.A.R., and M.A.M. were responsible for the conception and design of the experiments. F.G., K.F., and J.T. conducted the experiments. J.T., C.A.R., and M.A.M. performed sequence analysis and interpreted the results. C.A.R., M.H., and M.A.M. supervised the studies. J.T., and M.A.M. wrote the manuscript with support from all authors.

DECLARATION OF INTERESTS

J.T., F.G., K.F., M.H., C.A.R., and M.A.M. are employees of Ascend Advanced Therapies and have stock holdings in the company.

SUPPLEMENTAL INFORMATION

Supplemental information can be found online at https://doi.org/10.1016/j.omtm.2024.101384.

REFERENCES

1. Pupo, A., Fernández, A., Low, S.H., François, A., Suárez-Amarán, L., and Samulski, R.J. (2022). AAV vectors: The Rubik's cube of human gene therapy. Mol. Ther. *30*, 3515–3541. https://doi.org/10.1016/j.ymthe.2022.09.015.

2. Samulski, R.J., and Muzyczka, N. (2014). AAV-Mediated Gene Therapy for Research and Therapeutic Purposes. Annu. Rev. Virol. *1*, 427–451. https://doi.org/10.1146/annurev-virology-031413-085355.

3. FDA (2024). https://www.fda.gov/.

4. Reid, C.A., Hörer, M., and Mandegar, M.A. (2024). Advancing AAV production with high-throughput screening and transcriptomics. Cell & Gene Therapy Insights *10*, 821–840.

5. Kuzmin, D.A., Shutova, M.V., Johnston, N.R., Smith, O.P., Fedorin, V.V., Kukushkin, Y.S., van der Loo, J.C.M., and Johnstone, E.C. (2021). The clinical landscape for AAV gene therapies. Nat. Rev. Drug Discov. *20*, 173–174. https://doi.org/10.1038/d41573-021-00017-7.

6. Wang, J.-H., Gessler, D.J., Zhan, W., Gallagher, T.L., and Gao, G. (2024). Adeno-associated virus as a delivery vector for gene therapy of human diseases. Sig Transduct Target Ther *9*, 78. https://doi.org/10.1038/s41392-024-01780-w.

7. Chung, C.-H., Murphy, C.M., Wingate, V.P., Pavlicek, J.W., Nakashima, R., Wei, W., McCarty, D., Rabinowitz, J., and Barton, E. (2023). Production of rAAV By Plasmid Transfection Induces Antiviral and Inflammatory Responses in Suspension HEK293 Cells. Mol. Ther. Methods Clin. Dev. *28*, 272–283. https://doi.org/10.1016/j.omtm.2023.01.002.

8. Wright, J.F. (2023). AAV vector production: Troublesome host innate responses in another setting. Mol. Ther. Methods Clin. Dev. *28*, 412–413. https://doi.org/10.1016/j.omtm.2023.02.008.

9. Bennett, A., Mietzsch, M., and Agbandje-McKenna, M. (2017). Understanding capsid assembly and genome packaging for adeno-associated viruses. Future Virol. *12*, 283–297. https://doi.org/10.2217/fvl-2017-0011.

10. Onishi, T., Nonaka, M., Maruno, T., Yamaguchi, Y., Fukuhara, M., Torisu, T., Maeda, M., Abbatiello, S., Haris, A., Richardson, K., et al. (2023). Enhancement of recombinant adeno-associated virus activity by improved stoichiometry and homogeneity of capsid protein assembly. Mol. Ther. Methods Clin. Dev. *31*, 101142. https://doi.org/10.1016/j.omtm.2023.101142.

11. Srivastava, A., Mallela, K.M.G., Deorkar, N., and Brophy, G. (2021). Manufacturing Challenges and Rational Formulation Development for AAV Viral Vectors. J. Pharm. Sci. *110*, 2609–2624. https://doi.org/10.1016/j.xphs.2021.03.024.

12. Dumont, J., Euwart, D., Mei, B., Estes, S., and Kshirsagar, R. (2016). Human cell lines for biopharmaceutical manufacturing: history, status, and future perspectives. Crit. Rev. Biotechnol. *36*, 1110–1122. https://doi.org/10.3109/07388551.2015.1084266.

13. Tan, E., Chin, C.S.H., Lim, Z.F.S., and Ng, S.K. (2021). HEK293 Cell Line as a Platform to Produce Recombinant Proteins and Viral Vectors. Front. Bioeng. Biotechnol. *9*, 796991. https://doi.org/10.3389/fbioe.2021.796991.

14. Nguyen, T.N.T., Sha, S., Hong, M.S., Maloney, A.J., Barone, P.W., Neufeld, C., Wolfrum, J., Springs, S.L., Sinskey, A.J., and Braatz, R.D. (2021). Mechanistic model for production of recombinant adeno-associated virus via triple transfection of HEK293 cells. Mol. Ther. Methods Clin. Dev. *21*, 642–655. https://doi.org/10.1016/j.omtm.2021.04.006.

15. Berthet, C., Raj, K., Saudan, P., and Beard, P. (2005). How adeno-associated virus Rep78 protein arrests cells completely in S phase. Proc. Natl. Acad. Sci. USA *102*, 13634–13639. https://doi.org/10.1073/pnas.0504583102.

16. Hart, L.S., Ornelles, D., and Koumenis, C. (2007). The Adenoviral E4orf6 Protein Induces Atypical Apoptosis in Response to DNA Damage. J. Biol. Chem. *282*, 6061–6067. https://doi.org/10.1074/jbc.M610405200.

17. Milacic, M., Beavers, D., Conley, P., Gong, C., Gillespie, M., Griss, J., Haw, R., Jassal, B., Matthews, L., May, B., et al. (2024). The Reactome Pathway Knowledgebase 2024. Nucleic Acids Res. *52*, D672–D678. https://doi.org/10.1093/nar/gkad1025.

18. Wang, Y., Fu, Q., Lee, Y.S., Sha, S., and Yoon, S. (2023). Transcriptomic features reveal molecular signatures associated with recombinant adeno-associated virus production in HEK293 cells. Biotechnol. Prog. *39*, e3346. https://doi.org/10.1002/btpr.3346.

19. Junod, S.L., Saredy, J., and Yang, W. (2021). Nuclear Import of Adeno-Associated Viruses Imaged by High-Speed Single-Molecule Microscopy. Viruses *13*, 167. https://doi.org/10.3390/v13020167.

20. Nicolson, S.C., and Samulski, R.J. (2014). Recombinant Adeno-Associated Virus Utilizes Host Cell Nuclear Import Machinery To Enter the Nucleus. J. Virol. *88*, 4132–4144. https://doi.org/10.1128/JVI.02660-13.

21. Grafton, F., Feitzinger, R., Fisher, K., Leveque-Eichhorn, L., Reid, C.A., and Mandegar, M.A. (2023). A High-Throughput Small Molecule Screen Identifies Targets That Increase AAV9 Production in Suspension HEK293 Cells (ASGCT abstract 921). Mol. Ther. *31*, 4S1.

22. Barnes, C.R., Lee, H., Ojala, D.S., Lewis, K.K., Limsirichai, P., and Schaffer, D.V. (2021). Genome-wide activation screens to increase adeno-associated virus production. Mol. Ther. Nucleic Acids *26*, 94–103. https://doi.org/10.1016/j.omtn.2021.06.026.

23. Dreiman, G.H.S., Bictash, M., Fish, P.V., Griffin, L., and Svensson, F. (2021). Changing the HTS Paradigm: AI-Driven Iterative Screening for Hit Finding. SLAS Discov. *26*, 257–262. https://doi.org/10.1177/2472555220949495.

24. Yang, J., Grafton, F., Ranjbarvaziri, S., Budan, A., Farshidfar, F., Cho, M., Xu, E., Ho, J., Maddah, M., Loewke, K.E., et al. (2022). Phenotypic screening with deep learning identifies HDAC6 inhibitors as cardioprotective in a BAG3 mouse model of dilated cardiomyopathy. Sci. Transl. Med. *14*, eabl5654. https://doi.org/10.1126/scitranslmed.abl5654.

25. Higashino, F., Yoshida, K., Fujinaga, Y., Kamio, K., and Fujinaga, K. (1993). Isolation of a cDNA encoding the adenovirus E1A enhancer binding protein: a new human member of the ets oncogene family. Nucleic Acids Res. *21*, 547–553. https://doi.org/10.1093/nar/21.3.547.

26. Lipsick, J.S., and Baluda, M.A. (1986). The myb oncogene. Gene Amplif. Anal. *4*, 73–98.

27. Nakabeppu, Y., and Nathans, D. (1991). A naturally occurring truncated form of FosB that inhibits Fos/Jun transcriptional activity. Cell *64*, 751–759. https://doi.org/10.1016/0092-8674(91)90504-R.

28. Ryseck, R.P., Bull, P., Takamiya, M., Bours, V., Siebenlist, U., Dobrzanski, P., and Bravo, R. (1992). RelB, a new Rel family transcription activator that can interact with p50-NF-kappa B. Mol. Cell Biol. *12*, 674–684. https://doi.org/10.1128/mcb.12.2.674-684.1992.

29. Scarrott, J.M., Johari, Y.B., Pohle, T.H., Liu, P., Mayer, A., and James, D.C. (2023). Increased recombinant adeno-associated virus production by HEK293 cells using small molecule chemical additives. Biotechnol. J. *18*, 2200450. https://doi.org/10.1002/biot.202200450.

30. Wada, R. (2022). Enhancement of rAAV Productivity Utilizing HDAC Inhibitors on Helper-Free HEK293 Suspension Cell Culture Process (ASGCT abstract 766). Mol. Ther. *30*, 4S1.

31. Paszkiet, B.J., Zhang, J., Matukonis, M., Kaleko, M., and Luo, T. (2022). Histone Deacetylation Inhibitors Enhance Lentiviral Vector Production and Infectivity (Abstract 944). Mol. Ther. *5*, S308. https://doi.org/10.1016/S1525-0016(16)43774-3.

32. Gallinari, P., Di Marco, S., Jones, P., Pallaoro, M., and Steinkühler, C. (2007). HDACs, histone deacetylation and gene transcription: from molecular biology to cancer therapeutics. Cell Res. *17*, 195–211. https://doi.org/10.1038/sj.cr.7310149.

33. Lasorella, A., Benezra, R., and Iavarone, A. (2014). The ID proteins: master regulators of cancer stem cells and tumour aggressiveness. Nat. Rev. Cancer *14*, 77–91. https://doi.org/10.1038/nrc3638.

34. Sieweke, M.H., Tekotte, H., Frampton, J., and Graf, T. (1997). MafB represses erythroid genes and differentiation through direct interaction with c-Ets-1. Leukemia *11*, 486–488.

35. Bai, S., Shi, X., Yang, X., and Cao, X. (2000). Smad6 as a transcriptional corepressor. J. Biol. Chem. *275*, 8267–8270. https://doi.org/10.1074/jbc.275.12.8267.

36. Imamura, T., Takase, M., Nishihara, A., Oeda, E., Hanai, J., Kawabata, M., and Miyazono, K. (1997). Smad6 inhibits signalling by the TGF-β superfamily. Nature *389*, 622–626. https://doi.org/10.1038/39355.

37. Peng, Y., Kang, Q., Luo, Q., Jiang, W., Si, W., Liu, B.A., Luu, H.H., Park, J.K., Li, X., Luo, J., et al. (2004). Inhibitor of DNA Binding/Differentiation Helix-Loop-Helix Proteins Mediate Bone Morphogenetic Protein-induced Osteoblast Differentiation of Mesenchymal Stem Cells. J. Biol. Chem. *279*, 32941–32949. https://doi.org/10.1074/jbc.M403344200.

38. Yang, J., Li, X., Li, Y., Southwood, M., Ye, L., Long, L., Al-Lamki, R.S., and Morrell, N.W. (2013). Id proteins are critical downstream effectors of BMP signaling in human pulmonary arterial smooth muscle cells. Am. J. Physiol. Lung Cell Mol. Physiol. *305*, L312–L321. https://doi.org/10.1152/ajplung.00054.2013.

39. Franzoso, F.D., Seyffert, M., Vogel, R., Yakimovich, A., de Andrade Pereira, B., Meier, A.F., Sutter, S.O., Tobler, K., Vogt, B., Greber, U.F., et al. (2017). Cell Cycle-Dependent Expression of Adeno-Associated Virus 2 (AAV2) Rep in Coinfections with Herpes Simplex Virus 1 (HSV-1) Gives Rise to a Mosaic of Cells Replicating either AAV2 or HSV-1. J. Virol. *91*, e00357-17. https://doi.org/10.1128/JVI.00357-17.

40. DeLisle, A.J., Graves, R.A., Marzluff, W.F., and Johnson, L.F. (1983). Regulation of Histone mRNA Production and Stability in Serum-Stimulated Mouse 3T6 Fibroblasts. Mol. Cell Biol. *3*, 1920–1929. https://doi.org/10.1128/mcb.3.11.1920-1929.1983.

41. Polo, S.E., and Almouzni, G. (2005). Histone metabolic pathways and chromatin assembly factors as proliferation markers. Cancer Lett. *220*, 1–9. https://doi.org/10.1016/j.canlet.2004.08.024.

42. Ferreira, L.T., Figueiredo, A.C., Orr, B., Lopes, D., and Maiato, H. (2018). Dissecting the role of the tubulin code in mitosis. Methods Cell Biol. *144*, 33–74. https://doi.org/10.1016/bs.mcb.2018.03.040.

43. Shahid-Fuente, I.W., and Toseland, C.P. (2023). Myosin in chromosome organisation and gene expression. Biochem. Soc. Trans. *51*, 1023–1034. https://doi.org/10.1042/BST20220939.

44. Coplan, L., Zhang, Z., Ragone, N., Reeves, J., Rodriguez, A., Shevade, A., Bak, H., and Tustian, A.D. (2024). High-yield recombinant adeno-associated viral vector production by multivariate optimization of bioprocess and transfection conditions. Biotechnol. Prog. *40*, e3445. https://doi.org/10.1002/btpr.3445.

45. Ferreira, T.B., Perdigão, R., Silva, A.C., Zhang, C., Aunins, J.G., Carrondo, M.J.T., and Alves, P.M. (2009). 293 cell cycle synchronisation adenovirus vector production. Biotechnol. Prog. *25*, 235–243. https://doi.org/10.1002/btpr.64.

46. Wilkinson, M.G., and Millar, J.B. (2000). Control of the eukaryotic cell cycle by MAP kinase signaling pathways. FASEB J *14*, 2147–2157. https://doi.org/10.1096/fj.00-0102rev.

47. Zhang, W., and Liu, H.T. (2002). MAPK signal pathways in the regulation of cell proliferation in mammalian cells. Cell Res. *12*, 9–18. https://doi.org/10.1038/sj.cr.7290105.

48. Khan, N., Cheemadan, S., Saxena, H., Bammidi, S., and Jayandharan, G.R. (2020). MicroRNA-based recombinant AAV vector assembly improves efficiency of suicide gene transfer in a murine model of lymphoma. Cancer Med. *9*, 3188–3201. https://doi.org/10.1002/cam4.2935.

49. Balakrishnan, B., Sen, D., Hareendran, S., Roshini, V., David, S., Srivastava, A., and Jayandharan, G.R. (2013). Activation of the Cellular Unfolded Protein Response by Recombinant Adeno-Associated Virus Vectors. PLoS One *8*, e53845. https://doi.org/10.1371/journal.pone.0053845.

50. Foo, J., Bellot, G., Pervaiz, S., and Alonso, S. (2022). Mitochondria-mediated oxidative stress during viral infection. Trends Microbiol. *30*, 679–692. https://doi.org/10.1016/j.tim.2021.12.011.

51. Zhang, X., and Yu, W. (2022). Heat shock proteins and viral infection. Front. Immunol. *13*, 947789. https://doi.org/10.3389/fimmu.2022.947789.

52. Gano, J.J., and Simon, J.A. (2010). A Proteomic Investigation of Ligand-dependent HSP90 Complexes Reveals CHORDC1 as a Novel ADP-dependent HSP90-interacting Protein. Mol. Cell. Proteomics *9*, 255–270. https://doi.org/10.1074/mcp.M900261-MCP200.

53. Adachi, Y., Yamamoto, K., Okada, T., Yoshida, H., Harada, A., and Mori, K. (2008). ATF6 is a transcription factor specializing in the regulation of quality control proteins in the endoplasmic reticulum. Cell Struct. Funct. *33*, 75–89. https://doi.org/10.1247/csf.07044.

54. Zhang, R., Rapin, N., Ying, Z., Shklanka, E., Bodnarchuk, T.W., Verge, V.M.K., and Misra, V. (2013). Zhangfei/CREB-ZF - a potential regulator of the unfolded protein response. PLoS One *8*, e77256. https://doi.org/10.1371/journal.pone.0077256.

55. Liu, W., Baker, S.S., Baker, R.D., Nowak, N.J., and Zhu, L. (2011). Upregulation of Hemoglobin Expression by Oxidative Stress in Hepatocytes and Its Implication in Nonalcoholic Steatohepatitis. PLoS One *6*, e24363. https://doi.org/10.1371/journal.pone.0024363.

56. Schweitzer-Stenner, R. (2022). Heme–Protein Interactions and Functional Relevant Heme Deformations: The Cytochrome c Case. Molecules *27*, 8751. https://doi.org/10.3390/molecules27248751.

57. Espinoza, J.A., González, P.A., and Kalergis, A.M. (2017). Modulation of Antiviral Immunity by Heme Oxygenase-1. Am. J. Pathol. *187*, 487–493. https://doi.org/10.1016/j.ajpath.2016.11.011.

58. Kahlig, C.-I., Moser, S., Micutkova, L., Grillari, J., Kraus, B., and Hernandez Bort, J.A. (2024). Enhancement of rAAV titers via inhibition of the interferon signaling cascade in transfected HEK293 suspension cultures. Biotechnol. J. *19*, e2300672. https://doi.org/10.1002/biot.202300672.

59. Turner-Gillies, E., Shapiro, B., and Tian, F. (2024). Generation of Cell Lines Capable of Producing High-titer Viral Stocks for Use in Vaccine Manufacture and Gene Therapy. ATCC Application note. https://www.atcc.org/resources/application-notes/generation-of-cell-lines-capable-of-producing-high-titer-viral-stocks.

60. Galluzzi, L., Vitale, I., Aaronson, S.A., Abrams, J.M., Adam, D., Agostinis, P., Alnemri, E.S., Altucci, L., Amelio, I., Andrews, D.W., et al. (2018). Molecular mechanisms of cell death: recommendations of the Nomenclature Committee on Cell Death 2018. Cell Death Differ. *25*, 486–541. https://doi.org/10.1038/s41418-017-0012-4.

61. Strasser, L., Boi, S., Guapo, F., Donohue, N., Barron, N., Rainbow-Fletcher, A., and Bones, J. (2021). Proteomic Landscape of Adeno-Associated Virus (AAV)-Producing HEK293 Cells. Int. J. Mol. Sci. *22*, 11499. https://doi.org/10.3390/ijms222111499.

62. Ladd, B., Tunmats, S., Graslund, T., and Chotteau, V. (2024). Heterogeneity in Adeno-Associated Virus Transfection-Based Production Process Limits the Production Efficiency, ESACT Conference, Edinburgh, UK.

63. Andrews, S. (2010). FastQC: A Quality Control Tool for High Throughput Sequence Data [Online]. Available online at: http://www.bioinformatics.babraham.ac.uk/projects/fastqc/.

64. Kim, D., Paggi, J.M., Park, C., Bennett, C., and Salzberg, S.L. (2019). Graph-based genome alignment and genotyping with HISAT2 and HISAT-genotype. Nat. Biotechnol. *37*, 907–915. https://doi.org/10.1038/s41587-019-0201-4.

65. Liao, Y., Smyth, G.K., and Shi, W. (2014). featureCounts: an efficient general purpose program for assigning sequence reads to genomic features. Bioinformatics *30*, 923–930. https://doi.org/10.1093/bioinformatics/btt656.

66. Akhmedov, M., Martinelli, A., Geiger, R., and Kwee, I. (2020). Omics Playground: a comprehensive self-service platform for visualization, analytics and exploration of Big Omics Data. NAR Genom. Bioinform. *2*, lqz019. https://doi.org/10.1093/nargab/lqz019.

67. Subramanian, A., Narayan, R., Corsello, S.M., Peck, D.D., Natoli, T.E., Lu, X., Gould, J., Davis, J.F., Tubelli, A.A., Asiedu, J.K., et al. (2017). A Next Generation Connectivity Map: L1000 platform and the first 1,000,000 profiles. Cell *171*, 1437–1452.e17. https://doi.org/10.1016/j.cell.2017.10.049.